

# Mass spectrometric analysis and aerodynamic properties of various types of combustion-related aerosol particles

J. Schneider<sup>a,\*</sup>, S. Weimer<sup>a,1</sup>, F. Drewnick<sup>a</sup>, S. Borrmann<sup>a,b</sup>, G. Helas<sup>c</sup>, P. Gwaze<sup>c,2</sup>,  
O. Schmid<sup>c,3</sup>, M.O. Andreae<sup>c</sup>, U. Kirchner<sup>d</sup>

<sup>a</sup> Particle Chemistry Department, Max Planck Institute for Chemistry, P.O. Box 3060, 55020 Mainz, Germany

<sup>b</sup> Institute for Atmospheric Physics, Johannes Gutenberg University, 55099 Mainz, Germany

<sup>c</sup> Biogeochemistry Department, Max Planck Institute for Chemistry, P.O. Box 3060, 55020 Mainz, Germany

<sup>d</sup> Ford Research Center, Süterfeldstr. 200, 52072 Aachen, Germany

Received 6 April 2006; received in revised form 28 June 2006; accepted 10 July 2006

## Abstract

Various types of combustion-related particles in the size range between 100 and 850 nm were analyzed with an aerosol mass spectrometer and a differential mobility analyzer. The measurements were performed with particles originating from biomass burning, diesel engine exhaust, laboratory combustion of diesel fuel and gasoline, as well as from spark soot generation. Physical and morphological parameters like fractal dimension, effective density, bulk density and dynamic shape factor were derived or at least approximated from the measurements of electrical mobility diameter and vacuum aerodynamic diameter. The relative intensities of the mass peaks in the mass spectra obtained from particles generated by a commercial diesel passenger car, by diesel combustion in a laboratory burner, and by evaporating and re-condensing lubrication oil were found to be very similar. The mass spectra from biomass burning particles show signatures identified as organic compounds like levoglucosan but also others which are yet unidentified. The aerodynamic behavior yielded a fractal dimension ( $D_f$ ) of  $2.09 \pm 0.06$  for biomass burning particles from the combustion of dry beech sticks, but showed values around three, and hence more compact particle morphologies, for particles from combustion of more natural oak. Scanning electron microscope images confirmed the finding that the beech combustion particles were fractal-like aggregates, while the oak combustion particles displayed a much more compact shape. For particles from laboratory combusted diesel fuel, a  $D_f$  value of 2.35 was found, for spark soot particles,  $D_f \approx 2.10$ . The aerodynamic properties of fractal-like particles from dry beech wood combustion indicate an aerodynamic shape factor  $\chi$  that increases with electrical mobility diameter, and a bulk density of  $1.92 \text{ g cm}^{-3}$ . An upper limit of  $\chi \approx 1.2$  was inferred for the shape factor of the more compact particles from oak combustion.

© 2006 Elsevier B.V. All rights reserved.

**Keywords:** Aerosol mass spectrometry; Combustion aerosol; Aerodynamic properties; Aerosol chemistry

## 1. Introduction

Atmospheric aerosol particles generated by combustion sources do not only have a significant influence on atmospheric

chemistry, cloud processes and the Earth's climate, but can also affect human health. Combustion particles are produced by fossil fuel combustion (traffic, heating, and power generation) and biomass burning (natural forest or savanna fires, deforestation, wood burning, burning of agricultural wastes, etc.). Since combustion derived particles contain a significant amount of black carbon (BC), these particles have the potential to warm the atmosphere by absorption of short-wave solar radiation with subsequent re-emission of IR-radiation to the surrounding air [1,2]. However, this effect is strongly dependent on the single scattering albedo, a quantity that is highly uncertain for biomass burning particles [3], and therefore the whole issue of atmospheric warming by soot particles is currently under discussion [4]. On the other hand, combustion generated particles may act

\* Corresponding author. Tel.: +49 6131 305586; fax: +49 6131 305597.

E-mail address: [schneider@mpch-mainz.mpg.de](mailto:schneider@mpch-mainz.mpg.de) (J. Schneider).

<sup>1</sup> Present address: Laboratory of Atmospheric Chemistry, Paul Scherrer Institute, 5232 Villigen, and EMPA-Materials Science and Technology, Überlandstrasse 129, 8600 Dübendorf, Switzerland.

<sup>2</sup> Present address: Department of Geography, Environmental Management and Energy Studies, University of Johannesburg, P.O. Box 524, 2006 Auckland Park, South Africa.

<sup>3</sup> Present address: GSF-Research Center for Environment and Health, Institute for Inhalation Biology, P.O. Box 1129, 85758 Neuherberg, Germany.

as additional cloud condensation nuclei (CCN), leading to more but smaller cloud droplets and as a consequence to a delay of precipitation [5].

Epidemiological studies have provided evidence that elevated levels of ambient particulate concentration are associated with increased morbidity and mortality [6,7]. Although the exact pathophysiological pathways are still unknown [8] and studies focusing on ultrafine particles ( $d < 100$  nm, the typical size range of combustion particles) are sparse [9], human health is expected to be most affected by particles with aerodynamic diameters below about 200 nm, since these particles penetrate most efficiently into the alveolae [10]. In addition to the influences of particle size, number density, surface area, and volume, it is likely that potential health effects also depend on particle shape, chemistry, and hygroscopic properties, aspects that have been neglected in epidemiological studies [11].

Combustion derived particles consist of elemental carbon, unburned fuel components as observed in diesel exhaust particles [12–14], and chemical components that were produced during the combustion process and have condensed onto the particles, like polycyclic aromatic hydrocarbons (PAH) [15]. Biomass burning particles contain a significantly higher amount of organic carbon than elemental carbon [16], but can also contain inorganic material like sulfur species or potassium [17,18]. Similar to diesel exhaust particles, the organic compounds in biomass burning particles are mainly composed of unburned fuel and its pyrolysis products, which in this case are substances related to cellulose, like levoglucosan, etc. [16, and references therein].

The irregular, fractal-like shaped soot particles have aerodynamic properties that cannot be described in terms of “classical” aerosol mechanics with a simple, size-independent aerodynamic shape factor and an aerodynamic diameter. These particles are much better described in terms of fractal geometry, with the fractal dimension,  $D_f$ , being the characterizing quantity describing the degree of irregularity of the particles. There are numerous measurements of fractal dimensions of different types of agglomeration particles [e.g., 19–22], for particle sizes between 10 and 450 nm. Recently, DeCarlo et al. [23] and Slowik et al. [24] have demonstrated the ability to infer particle morphology and density from simultaneous measurements of the vacuum aerodynamic diameter,  $d_{va}$ , measured by the aerodyne aerosol mass spectrometer (AMS) and the mobility diameter,  $d_m$ , measured by a differential mobility analyzer (DMA) for electrical mobility diameters between 100 and 400 nm.

The AMS has recently been used for various studies of engine exhaust particles [12,13]. The detection process of the AMS relies on flash evaporation of the non-refractory compounds on a hot surface at temperatures around 400–700 °C. This excludes the detection of pure soot, since elemental carbon does not evaporate at these temperatures. However, despite the fact that the AMS cannot detect the elemental carbon in soot particles directly, it can detect condensed substances on these particles, and therefore this instrument can be used for studies of combustion exhaust particles including the aerodynamic properties of these particles. This coating may contain organic or inorganic low-volatile combustion products, but also contamination

from organic substances formed during particle production and sampling in the laboratory. Although it is only the coating of the soot particles from which composition mass spectra are obtained in this study, the aerodynamic sizing performed by the AMS drift region pertains to the entire particle including the soot and volatile components. This paper reports on mass spectrometric measurements of the non-refractory components of a variety of combustion particles, summarizing several field and laboratory studies from the last 5 years. In the first part, we compare the mass spectra obtained from diesel combustion particles, spark-discharge generated graphite particles, biomass burning aerosol and particles generated with various fuel types using a laboratory burner. In the second part, we use the relation between the vacuum aerodynamic diameter ( $d_{va}$ ) and the electrical mobility equivalent diameter ( $d_m$ ) in order to infer the fractal dimension, the dynamic shape factor, the effective density, and the bulk density of particles in the size range between 100 and 850 nm.

## 2. Aerodynamic sizing of fractal-like particles

### 2.1. General

The aerodynamic sizing in the aerodyne AMS (as well as in most other aerosol mass spectrometers) utilizes the acceleration of the particles while entering the high vacuum chamber. This acceleration occurs during the expansion at the last orifice of the aerodynamic lens into the vacuum chamber. The aerodynamic lens operates at pressures of typically 1–2 hPa, therefore the particles travel in the free molecular flow regime [25]. The ‘classical’ aerodynamic diameter  $d_a$ , which is defined for the continuum flow regime, is related to the volume equivalent diameter  $d_{ve}$  (the diameter of a sphere that has the same volume as the non-spherical particle) by the following equation:

$$d_a^2 = \frac{\rho_p}{\rho_0} \frac{1}{\chi} d_{ve}^2 \frac{C_c(Kn(d_{ve}))}{C_c(Kn(d_a))}, \quad (1)$$

where  $\rho_p$  denotes the particle bulk density,  $\rho_0$  the unit density ( $1 \text{ g cm}^{-3}$ ),  $\chi$  the dynamic shape factor,  $C_c(Kn)$  the Cunningham slip correction, and  $Kn(d) = 2\lambda/d$  is the Knudsen number for particles with diameter  $d$  [26], with  $\lambda$  the mean free path of air molecules. The dynamic shape factor  $\chi$  equals unity for spherical particles and is larger than 1 for non-spherical particles. In the free molecular flow regime, the Cunningham slip correction factor is inversely proportional to the particle diameter [27], leading to the so-called “vacuum aerodynamic diameter”  $d_{va}$ :

$$d_{a,\text{free molecular}}^2 = d_{va}^2 = \frac{\rho_p}{\rho_0} \frac{1}{\chi} d_{ve}^2 \frac{d_{va}}{d_{ve}} \Rightarrow d_{va} = \frac{\rho_p}{\rho_0} \frac{1}{\chi} d_{ve} \quad (2)$$

which is defined as the aerodynamic diameter in the free molecular flow regime [e.g., 25,28].

A differential mobility analyzer measures the “electrical mobility equivalent diameter”  $d_m$ , which is related to the vacuum aerodynamic diameter by

$$\frac{d_{va} \chi^2 \rho_0}{\rho_p C_c(d_{va} \chi \rho_0 / \rho_p)} = \frac{d_m}{C_c(d_m)} \quad (3)$$

Up to here, we assumed for simplicity that the dynamic shape factor in the transition regime ( $\chi_t$ ) and in the free molecular regime ( $\chi_{va}$ ) are equal. However, especially for fractal-like particles, the difference between  $\chi_t$  and  $\chi_{va}$  may become important [23].

By combining a DMA and an AMS, only the parameters  $d_m$  and  $d_{va}$  are measured, so that Eq. (5) cannot be easily used to infer the particle density or shape factor. Frequently, an effective density is introduced, although there are different definitions for it [23]. Here, we will use the effective density defined by:

$$\rho_{\text{eff}} = \rho_0 \frac{d_{va}}{d_m} = \rho_p \frac{C_c(d_{va}\chi\rho_0/\rho_p)}{\chi^2 C_c(d_m)} \quad (4)$$

Since the DMA operates under ambient pressure conditions, the particles inside the DMA are in the transition between the free molecular and the continuum regime. Following Jimenez et al. [25], the following approximate expression for the Cunningham correction  $C_c$  in the transition regime can be used with an error smaller than 10% for Knudsen numbers between 0.01 and 100:

$$C_c = 1 + \Phi Kn, \quad (5)$$

where  $\Phi = 1.594$  is an empirical constant. Inserting Eq. (5) into Eq. (6) gives an equation that is quadratic in  $\rho_{\text{eff}}$ . Solving for  $\rho_{\text{eff}}$  yields:

$$\rho_{\text{eff}} = \frac{\rho_p}{\chi^2} \frac{1}{2(1+\Phi(2\lambda/d_m))} \left[ 1 + \sqrt{1 + \frac{8\chi\Phi\lambda(1+\Phi(2\lambda/d_m))}{d_m}} \right]. \quad (6)$$

## 2.2. Fractal-like particles

The fractal dimension of an agglomerate of primary particles describes the relationship between its geometric extension and the number of primary particles:

$$N_{pp} \propto R^{D_f} \quad (7)$$

where  $N_{pp}$  is the number of primary particles,  $D_f$  the fractal dimension, and  $R$  is the characteristic radius (radius of gyration) of the agglomerate [29].  $D_f$  varies between 1 and 3, with an infinitely long change-like aggregate and a solid sphere as limiting cases, respectively. The scaling laws for fractal-like particles that were developed by Schmidt-Ott et al. [30] led to the mass–mobility relationship [31] that relates the total particle mass  $m_p$  to the ratio between the electrical mobility diameter ( $d_m$ ) and the diameter of the primary particles ( $d_{pp}$ ) by the fractal dimension:

$$m_p \propto \left( \frac{d_m}{d_{pp}} \right)^{D_f} \quad (8)$$

Considering that in the free molecular regime,  $d_{ve}^2 = d_m^2/\chi_{va}$  (following from Eqs. (2) and (4)) and  $d_{ve} = \chi_{va}d_{va}\rho_0/\rho_p$  (Eq. (3)), we can express the total particle mass by:

$$m_p = \frac{\pi}{6} \rho_p d_{ve}^3 = \frac{\pi}{6} \rho_p \frac{d_m^2}{\chi_{va}} \chi_{va} \frac{\rho_0}{\rho_p} d_{va} = \frac{\pi}{6} \rho_0 d_m^2 d_{va}. \quad (9)$$

Combining Eqs. (8) and (9), and assuming that  $d_{pp}$  is a constant, it follows that  $d_{va}$  and  $d_m$  are related by:

$$d_{va} = C d_m^{D_f-2}, \quad (10)$$

where  $C$  is a constant. van Gulijk et al. [32] point out that in the free molecular regime, for particles with fractal dimensions smaller than 2, both the aerodynamic and the mobility diameter are independent of  $D_f$ . As a consequence, only fractal dimensions larger than 2 can be determined from simultaneous measurements of  $d_{va}$  and  $d_m$ . An additional constraint is the requirement that  $d_{pp}$  is a constant value.  $d_{pp}$  can be determined by sampling the particles on a filter and measuring the size of the primary particles using electron microscopy. If such information is available, Eq. (10) can be applied in order to infer the fractal dimension of the measured particles. This method has been applied to diesel soot particle data obtained with a DMA and an electrical low pressure impactor (ELPI) by van Gulijk et al. [32], and for propane flame soot data measured with an AMS and a DMA by Slowik et al. [24].

## 3. Measurements

### 3.1. Instrumentation

The aerodyne aerosol mass spectrometer, which has been previously described by several authors [e.g., 12,25,33–36] uses a combination of aerodynamic focusing and sizing, thermal vaporization (400–700 °C), electron impact ionization, and mass spectrometric detection to infer quantitative chemical composition as well as chemically resolved size distributions of aerosol particles in the aerodynamic size range between 25 and 1500 nm. In the experiments presented here, the instrument was equipped with a linear quadrupole mass spectrometer. The vacuum aerodynamic diameter measurement was calibrated with ammonium nitrate and ammonium sulfate particles that were size-selected with a DMA, and with polystyrene latex (PSL) spheres of known diameters between 50 and 600 nm. The data presented here originate from three different experimental settings, namely laboratory, biomass combustion facility, and a chassis dynamometer car testing facility. The DMA systems employed in the experiments were TSI models 3071 and 3080, the condensation particle counters were TSI models 3025a and 3022.

### 3.2. Fuel combustion and soot aerosol generation in the laboratory

Combustion particles were generated in the laboratory by burning diesel and gasoline in a commercial camping burner. This burner can be operated at different air-to-fuel ratios, thereby varying the flame type and color from oxygen-rich (blue) to oxygen-poor (yellow). To maintain a stable airflow around the burner, a steel flow chamber (diameter: 200 mm; height: 500 mm) was placed around the burner. The stainless steel sampling line to the AMS and the DMA extracted the aerosol from the flow chamber 15 cm above the burner exit. Connections between the stainless steel tube, the AMS and the DMA were

made of conductive silicone tubing, which turned out to be a source of contamination. Particles generated in the blue flame had a modal vacuum aerodynamic diameter,  $d_{va}$  (mass based) of about 60 nm, the particles from the yellow flame had a modal  $d_{va}$  between 120 and 180 nm.

The different fuel types were also nebulized unburned using a De Vilbiss-type nebulizer [26] for subsequent analysis with the AMS. Lubrication oil droplet aerosol also was produced by heating the oil to 120 °C, leading to evaporation and re-condensation of the higher volatile fraction of the oil. In addition, airborne graphite soot particles, generated by a PALAS GFG-100 spark soot generator using Argon as a carrier gas [37,38], were subjected to AMS measurements.

### 3.3. Biomass burning aerosol generation

The biomass burning facility of the Max Planck Institute for Chemistry has been described in detail in Gwaze et al. [22] and Iinuma et al. [39]. Various types of wood, such as beech, oak, musasa (*Brachystegia speciformis*), spruce, and other biomass burning material (savanna grass) were burned on a fuel bed housed in a partially closed container open to ambient air. The smoke was conducted into a dark reservoir container (32 m<sup>3</sup>), from which the aerosol instruments were sampling. The beech wood consisted of dry sticks from a hardware store with a length of about 15 cm and a thickness of 0.5 cm, while the other biomass fuels were in a natural state.

### 3.4. Measurements of diesel exhaust from a passenger car

The diesel engine exhaust measurements were performed at the chassis dynamometer of the Ford Research Center Aachen (FFA). A detailed description of these measurements is given in Schneider et al. [13] and Scheer et al. [40]. The exhaust of a diesel passenger car was sampled through stainless steel tubing and diluted with particle free air with dilution factors varying between 10 and 300. A scanning mobility particle sizer and a condensation particle counter were run parallel to the AMS. Here, we present an example of the mass spectrometric data (engine condition: 6 kW, 120 km h<sup>-1</sup>). Overall results and details from these studies have been presented in Schneider et al. [13] and Scheer et al. [40].

## 4. Results and discussion

### 4.1. Mass spectra of combustion derived particles

Fig. 1 depicts mass spectra of particles produced from diesel and lube oil by combustion, nebulization, and evaporation with subsequent re-condensation. Panel A shows a typical AMS mass spectrum of particles from laboratory combusted diesel (oxygen-rich blue flame, height of sampling tube: 15 cm above flame; AMS vaporizer temperature: 412 °C). Panel B shows a mass spectrum from particles sampled behind the exhaust pipe of a diesel passenger car (conditions: 6 kW, 120 km h<sup>-1</sup>). Only the organic signatures are shown in this mass spectrum, while the sulfate signals were subtracted, since the latter are from

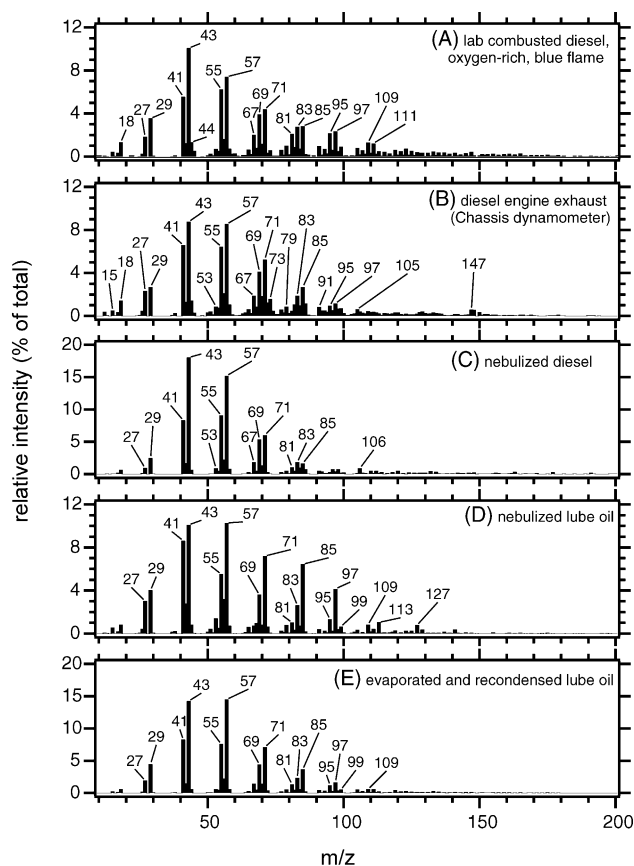


Fig. 1. Comparison of mass spectra of particles derived from diesel combustion in the laboratory burner (A) with those of particles from diesel engine exhaust (B), from nebulized diesel (C), nebulized lube oil (D), and evaporated and re-condensed lube oil (E).

sulfate aerosol that is formed due to conversion of gaseous SO<sub>2</sub> into SO<sub>3</sub> at the oxidation catalyst of the car [13]. This does not occur in the laboratory generated diesel combustion particles. Panel C shows a mass spectrum from nebulized diesel (vaporizer temperature: 446 °C), panels D and E show two mass spectra from lube oil, nebulized (D) and evaporated at 120 °C with subsequent re-condensation (E). Both lube oil mass spectra were recorded with a vaporizer temperature of 480 °C.

Mass spectrum A is dominated by hydrocarbon fragment ions like C<sub>n</sub>H<sub>2n-1</sub><sup>+</sup> ( $m/z = 27, 41, 55, 69, 83, 97, 111, \dots$ ), C<sub>n</sub>H<sub>2n+1</sub><sup>+</sup> ( $m/z = 29, 43, 57, 71, 85, 99, \dots$ ), and C<sub>n</sub>H<sub>2n-3</sub><sup>+</sup> (67, 81, 95, 109, ...). Also, CO<sub>2</sub><sup>+</sup> ( $m/z = 44$ ) and H<sub>2</sub>O<sup>+</sup> ( $m/z = 18$ ) are detected, both of which are fragments of larger organic molecules. The diesel exhaust particle mass spectrum (panel B of Fig. 1) shows similar mass fragments, but ions with  $m/z$  numbers larger than 100 are less abundant. Also, the relative amount of other fragments with even  $m/z$  numbers (e.g., 82, 84, and 96) is higher compared to their “neighbor” ions (83, 85, and 97). The signals at  $m/z$  73 or 147 are possibly due to contamination arising from the conductive silicone tubing, as it is reported that dimethylsiloxane, SiO(CH<sub>3</sub>)<sub>2</sub>, which as a polymer with the empirical formula [SiO(CH<sub>3</sub>)<sub>2</sub>]<sub>n</sub> is popularly known as silicone) produces mass peaks at  $m/z$  73, 147, 207, 221, and 281 under electron ionization [41].

The nebulized diesel (panel C) shows similar signatures with respect to the three ion series  $C_nH_{2n-1}^+$ ,  $C_nH_{2n+1}^+$ , and  $C_nH_{2n-3}^+$ , and the peaks with even mass numbers (80, 82, 84, etc.) are very small.

The mass spectra from lubrication oil (panels D and E) show also the three ion series, but the ionic fragments are larger than in the mass spectrum of particles from nebulized diesel. Especially the mass spectrum from nebulized lube oil shows larger ionic fragments and more intense peaks with even  $m/z$  values (e.g., 42 and 56) than in the mass spectrum from evaporated and re-condensed oil lube droplets. Also, there are peaks at  $m/z$  113 and 127, which are only found in the nebulized lube oil. This finding is due to the fact that the nebulization process transforms the complete mixture of substances that is contained in the lubrication oil into droplets, while the evaporation and re-condensation process enriches the higher volatile compounds in the droplets.

The similarities between the mass spectra shown in Fig. 1 can be compared by plotting the relative intensities of the individual  $m/z$  values against each other (see Fig. 2). The mass spectrum of diesel engine exhaust particles was arbitrarily chosen as the reference mass spectrum. The correlation coefficient  $r$  (also called Pearson's  $r$ ) of the linear fit is used here as measure of similarity between the individual mass spectra, a method that has been used previously [46]. For two identical mass spectra, the intensities of the individual mass peaks fall onto a straight line with an  $r$  value of 1. For mass spectra that are not identical, the data points deviate from that line, resulting in a correlation coefficient smaller than 1. Note that the  $r^2$  value is not suited

for this method, since a negative correlation ( $r = -1$ , but  $r^2 = 1$ ) indicates a pronounced difference between two mass spectra. Fig. 2 shows that the AMS mass spectra of lab combusted diesel particles and evaporated and re-condensed lube oil particles have the highest similarity to those of diesel exhaust particles from the passenger car, suggesting that the higher volatile components of the lubrication oil or the diesel fuel are more likely to evaporate during the combustion process and to condense unburned onto the soot particles. However, these differences between the correlation coefficients are small, since  $r$  varies only between 0.95 and 0.97. Canagaratna et al. [12] came to a similar result when comparing heavy-duty diesel exhaust particles to nebulized diesel fuel particles and evaporated/re-condensed lubrication oil particles. Investigating also heavy-duty diesel exhaust particles, Tobias et al. [42] found that at low engine loads, the exhaust particle composition is similar to that of diesel fuel, but for higher loads the composition is indicative of lubricating oil. In contrast, Sakurai et al. [43] found that heavy-duty engine exhaust particles are dominated (>80%) by lubrication oil. For a non-road diesel generator, Liang et al. [44] concluded from their data that the exhaust particles contain  $n$ -alkanes that are likely from unburned diesel fuel, while the main source of organic acids is lubrication oil. The various data sets suggest that diesel exhaust particles are composed of a mixture of fuel and lubrication oil compounds, and that engine type and load determine if one of the components dominates. Our investigation with laboratory burned diesel fuel further indicates that also the combustion of pure diesel fuel (without addition of lubrication oil) produces particles that are similar to those observed in diesel

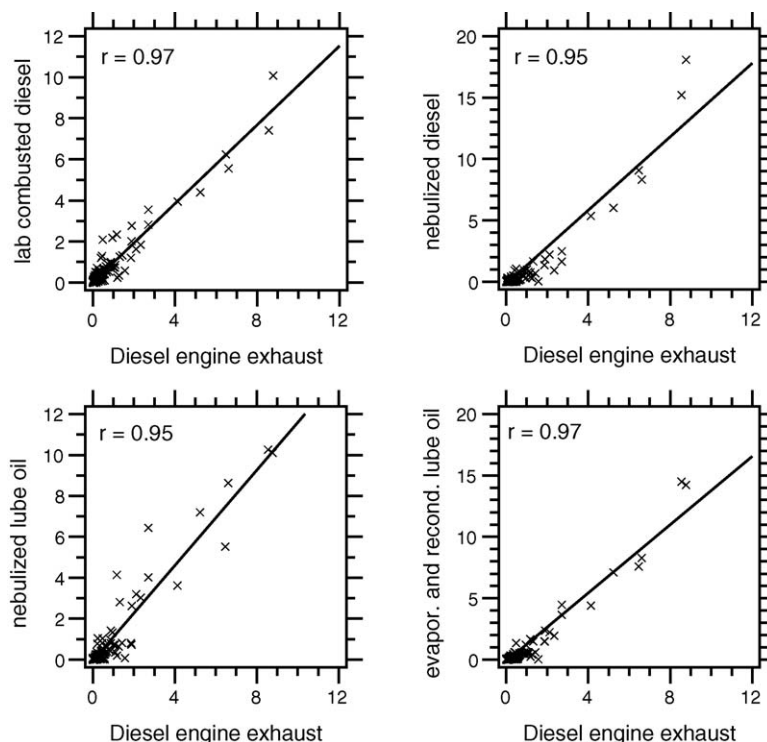


Fig. 2. Correlation plots of the mass spectra displayed in Fig. 1. Plotted are the intensities of the individual  $m/z$  signals against each other. The correlation coefficient  $r$  is used here as a measure of similarity between the spectra.

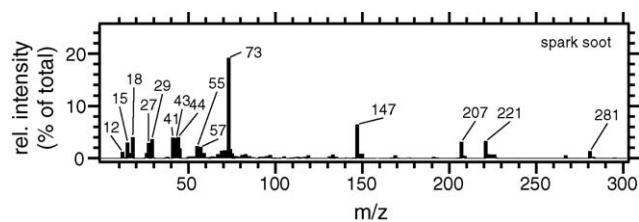


Fig. 3. Mass spectrum of particles generated by the spark snot generator. The observed mass peaks are likely due to contamination:  $m/z$  27, 29, 41, 43, 55, and 57 from the discharge chamber of the generator [38] and  $m/z$  73, 147, 207, 221, and 281 from the conductive silicone tubing [41]. However, these contamination signals can be used to infer the size distribution of the snot particles with the AMS.

exhaust. Thus, we cannot distinguish whether the refractory parts of diesel engine exhaust particles are composed of diesel fuel or the higher volatile fraction of lube oil, since both types of substances lead to particles that reveal similar mass spectra.

Fig. 3 depicts a mass spectrum of snot particles produced by the spark snot generator. Although these particles are supposed to consist of pure elemental carbon [37] and should therefore not be vaporized by the AMS vaporizer, several distinct peaks are observed, namely at  $m/z$  = 27, 29, 41, 43, 55, and 57 ( $C_nH_{2n-1}^+$ ,  $C_nH_{2n+1}^+$ ), and at  $m/z$  = 73, 147, 207, 221, and 281. These mass peaks indicate organic contamination of the snot particles produced by the spark discharge generator. Roth et al. [38] also found that snot particles produced with the PALAS CFG-1000 generator contained up to 25% volatile contamination. They concluded that these contaminations were due to organics evaporating from the walls of the polyamide chamber of the generator. The observed ions  $C_nH_{2n-1}^+$ ,  $C_nH_{2n+1}^+$  are most likely due to this contamination source. The signals at  $m/z$  73, 147, 207, 221, and 281 are likely due to contamination from conductive silicone tubing, a material that is commonly used in aerosol science. McLafferty and Turecek [41] report exactly these mass peaks as signatures for dimethylsiloxane which is the constituent of the polymeric substance commonly known as silicone. These ions can be identified with  $(SiOC_2H_6)_nSiOC_2H_5^+$  ( $n=0$ ,  $m/z$  73;  $n=1$ ,  $m/z$  147;  $n=2$ ,  $m/z$  221;  $n=3$ ,  $m/z$  295),  $(SiOC_2H_6)_2SiOCH_3^+$ :  $m/z$  207, and  $(SiOC_2H_6)_3SiOCH_3^+$ :  $m/z$  = 281. It is interesting to note that these signatures did not occur when the laboratory generated blue diesel flame was probed, but occurred only when the yellow (oxygen-poor) flame was measured where snot production was observed. It appears that the silicone components preferably condense on or react with snot particles. Although this contamination is undesired, it allows the detection of the spark snot particles with the AMS, and thereby the measurement of the vacuum aerodynamic diameter of the spark snot particles (Section 4.2).

Fig. 4 gives several examples of biomass burning derived particles: panel A shows a mass spectrum of particles produced by dry beech wood combustion. Besides the ion series ( $C_nH_{2n-1}^+$ ,  $C_nH_{2n+1}^+$ , and  $C_nH_{2n-3}^+$ ), these particles also contain the silicone contamination products  $m/z$  73, 147, 207, and 221, but also  $m/z$  167 and 181, two yet unidentified ions.

The biomass burning particle mass spectra also contain  $m/z$  60, which is assumed to be a signature of levoglucosan

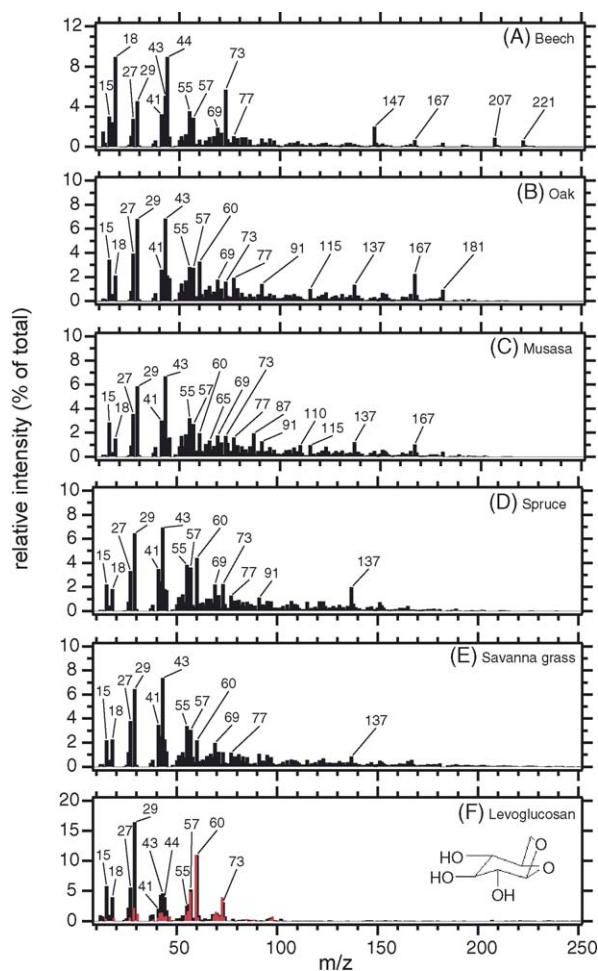


Fig. 4. Mass spectra from various biomass burning derived particles (panels A–E), along with a laboratory spectrum of levoglucosan (panel F, black trace) and the NIST reference spectrum (panel F, red trace).

(1,6-anhydro- $\beta$ -D-glucopyranose,  $C_6H_{10}O_5$ , molecular weight (MW)  $162\text{ g mol}^{-1}$ ), a thermal decomposition product of cellulose constituents that is ubiquitous found in biomass burning particles (e.g., [16, and references therein]). To test this hypothesis, levoglucosan, dissolved in water, was nebulized in the laboratory and analyzed with the AMS (panel F). It was found that levoglucosan produces a significant mass peak at  $m/z$  60, but also produces  $m/z$  73, while no  $m/z$  147, 207, 221, and 281 are observed. The NIST standard reference mass spectrum of levoglucosan [45] is also given in panel F (red trace). The main fragment ions of levoglucosan ( $m/z$  57 ( $C_4H_9^+$  or more likely  $C_3H_5O^+$ ),  $m/z$  60 ( $C_2H_4O_2^+$ ), and  $m/z$  73 ( $C_3H_5O_2^+$ ) are produced in the AMS mass spectrum at similar ratios as in the NIST reference spectrum. The signal ratio of  $m/z$  57: $m/z$  60: $m/z$  73 is 0.44:1:0.36 (NIST) and 0.48:1:0.28 (AMS) which can be considered as close agreement. The mass spectrum of the AMS was recorded with a vaporizer temperature of  $430\text{ }^\circ\text{C}$ , and the ratios change in favor of the smaller fragments with increasing vaporizer temperature, but the signatures of  $m/z$  60 and 73 remain. The smaller ion fragments that were produced in the AMS ( $m/z$  15, 18, 27, 29, 41, 43, 44, etc.) to a higher degree than in the NIST spectrum are most likely also caused by fragmentation

or vibrational excitation during the flash vaporization process. This finding is consistent with previous comparisons of AMS and NIST mass spectra from various organic compounds [46]. There are also other substances in the NIST database similar to levoglucosan (e.g., D-arabinose or D-ribose, both  $C_5H_{10}O_5$ , MW 150) that produce peaks at  $m/z$  60 and 73, as also do long-chain carboxylic acids (starting with heptanoic acid,  $C_7H_{14}O_2$ , MW 130). Since organic acids have been found previously in biomass burning particles [16], it would not be unlikely that the detection of  $m/z$  60 and 73 might also be explained by carboxylic acids, but the peak ratios of  $m/z$  57: $m/z$  60: $m/z$  73 do not match the values found in the biomass burning particles.

The ratio  $m/z$  60 to  $m/z$  73 observed in the levoglucosan mass spectrum allows to distinguish between the  $m/z$  73 signature due to levoglucosan production and due to silicone contamination: for example, the beech spectrum (panel A) contains an intense signal at  $m/z$  73 but only low signal at  $m/z$  60, indicating that most of  $m/z$  73 is due to contamination in panel A, while in the spruce mass spectrum (panel D) the ratio between 60 and 73 is very similar to that observed in the levoglucosan spectrum. Levoglucosan does not produce a peak at  $m/z$  137, which is very pronounced in the mass spectra of oak (B), musasa (C), spruce (D), and savanna grass (E), but not in the beech spectrum (A).  $m/z$  167 and 181, on the other hand are most intense in the mass spectra from beech (A), oak (B), and musasa (C). Since these  $m/z$  ratios are separated by 14 mass units, they belong most likely to the same ionic fragmentation chain, with different numbers of  $CH_2$ -groups. A similar relationship may exist between  $m/z$  137 and 151.

Bahreini et al. [47] presented an AMS mass spectrum of particles from an ambient brush fire plume, in which no prominent mass peaks are observed at  $m/z$  larger than 70, but the data are only displayed up to an  $m/z$  value of 100. Thus, it cannot be assessed if the mass spectrum of these ambient brush fire plume particles contains ions at  $m/z$  137, 157, and 181.  $m/z$  60 and 73 are definitely minor peaks in the mass spectrum of Bahreini et al., while  $m/z$  44 ( $CO_2^+$ ) is a very pronounced peak, almost as prominent as the peak at  $m/z$  29 ( $C_2H_5^+$ ). The latter is the most intense peak in the brush fire mass spectrum. In our data,  $m/z$  44 is the most prominent peak only in Fig. 4A (beech sticks), while the other mass spectra from biomass burning derived particles reveal a higher intensity at  $m/z$  43 and at  $m/z$  29 than at  $m/z$  44. The particle size distribution recorded simultaneously shows that the  $CO_2^+$  signal is not due to gas phase  $CO_2$ , since gas molecules arrive much faster at the ionizer of the AMS than particles and can thereby be distinguished from the particle phase. The ratio of  $m/z$  44 to total organics has been used to infer the degree of processing that the organic aerosol particles or their organic precursor gases have experienced in the atmosphere. It has been found that in remote, rural areas  $m/z$  44 is the highest peak in the organic mass spectrum [46,48], and it was concluded that  $m/z$  44 is a reliable marker for the occurrence of oxygenated organic aerosol (OOA) [49]. Takegawa et al. [50] used the ratio of  $m/z$  44 to total organics to assess the degree of processing of organic aerosols, and used for Tokyo city thresholds of 0.04 and 0.08 to separate between low, moderately, and highly processed aerosol, respectively.

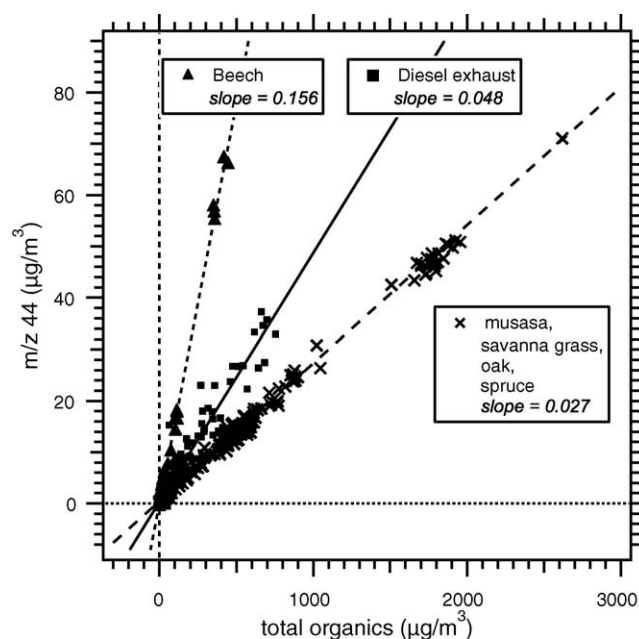


Fig. 5.  $m/z$  44 mass concentration vs. total organic mass concentrations, for data obtained from diesel exhaust particles and biomass burning particles.

Fig. 5 shows the mass concentration of  $m/z$  44 plotted versus the total organic mass concentration for the biomass burning and diesel exhaust data. The identified contamination products were subtracted from the organic signal for this analysis. Interestingly, the biomass burning data fall in two distinct groups. The beech combustion derived data reveal a markedly higher slope (0.156) than the other biomass derived particles (oak, musasa, spruce, and savanna grass combustion), which all fall onto a single regression line with a slope of 0.027. The diesel exhaust data (recorded at the chassis dynamometer during two different campaigns) show a slope of 0.048.

The very low ratio of  $m/z$  44 to total organics of the biomass burning derived particles from natural fuel is surprising, since it was expected that this ratio reflects the degree of oxidation of the organic compounds. Results obtained from chemical analysis of biomass burning aerosol show a large fraction of oxygen containing compounds and functional groups [17,39]. This finding suggests that the method of determining the degree of oxidation using the ratio of  $m/z$  44 intensity to total organic peak intensity may not be universally applicable to all oxygenated organic molecules. This is illustrated in the relatively low intensity of  $m/z$  44 in the highly oxygenated compound, levoglucosan: the measured ratio of  $m/z$  44 to total organics for levoglucosan inferred from our laboratory experiments is 0.056. For example, since  $m/z$  43 can also contain fragments of oxygen-containing organic species ( $C_2H_3O^+$ ), the structure of certain oxygenated molecules may lead to a stronger formation of  $m/z$  43 instead of  $m/z$  44 during the vaporization and ionization process inside the AMS.

It must be emphasized that the beech wood was dry beech sticks from a hardware store, while the other biomass fuel was in an almost natural state and thereby contained much more water. Biomass burning particles from natural wood (e.g., forest fires)

are more likely to resemble the “low slope” data, while modern wood-based heating systems (e.g., wood pellets) will resemble the dry beech wood. Therefore, one has to distinguish between these different types of biomass burning and the ratio of  $m/z$  44 to total organics alone cannot be used to unambiguously infer the type of fuel. These differences between the different types of biomass burning particles also appear in their aerodynamic properties which will be discussed in the following section.

#### 4.2. Aerodynamic properties and fractal dimension

To infer information about the aerodynamic properties as well as density and shape of the particles, a narrow size range of the sampled aerosol was selected using a DMA and the resulting particles were analyzed with the AMS, giving information on the vacuum aerodynamic particle diameter. Multiply charged particles that appeared at a higher vacuum aerodynamic diameter than the singly charged ones were excluded from the analysis. These data are available from the following experiments: biomass burning (oak and beech), graphite soot from the spark soot generator, and lab combusted diesel particles (oxygen-poor flame).

Fig. 6 shows the relationship between the mobility diameter (selected with the DMA) and the vacuum aerodynamic diameter (measured with the AMS) for particles obtained from two types of wood burning: dry beech sticks and natural oak branches. The measurements show a significantly different behavior; while for the particles from beech combustion, the vacuum aerodynamic diameter shows only a very slight dependence on the mobility diameter, the vacuum aerodynamic diameter of the particles from oak combustion is linearly dependent on the mobility diameter.

As explained above, the relation of the measured diameters  $d_{va}$  and  $d_m$  (Eq. (10)) can be used to infer the fractal dimension  $D_f$  of the particles. The diameter of the primary particles from beech combustion was measured by Gwaze et al. [22] using

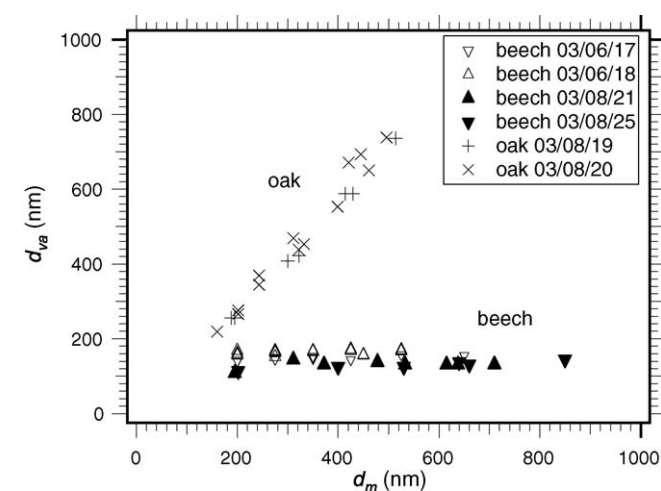


Fig. 6. Vacuum aerodynamic diameter vs. mobility equivalent diameter for two types of biomass burning aerosol: oak, measured on August 19 and 29, 2003 (crosses), and beech, measured on June 17 and 18, and August 21 and 25, 2003 (triangles).

scanning electron microscopy. They found a constant Gaussian distribution of the primary particle diameter  $d_{pp}$  with a modal diameter of 51 nm and a standard deviation  $\sigma_g$  of 1.27. We will therefore assume a constant  $d_{pp}$  and apply Eq. (10) to our data in order to infer the fractal dimension of the measured particles.

When plotting the logarithms of the data, the slope of a linear regression line equals  $D_f - 2$ . This has been done separately for the individual experiments shown in Fig. 7, each containing between 6 and 32 data points. We obtain fractal dimensions between 3.06 and 3.09 for the particles from oak combustion, and fractal dimensions between 2.04 and 2.15 for the particles derived from beech combustion.

##### 4.2.1. Statistical significance of the fractal dimension data

In order to test the statistical significance of the positive correlations that were found for the data presented in Fig. 7, we used the Student's  $t$ -test. This test yielded statistical significance within the 95% confidence interval for all experiments with the exception of the beech wood experiment of 03/08/21, where the correlation coefficient is as low as 0.52 and also the number of data points (8) is low. Within the 99% confidence level, still the two oak experiments and the beech experiment of 03/08/25 are statistically significant. Since the value obtained from the experiment on 03/08/21 is not even significant within the 90% confidence level, we exclude this data point from the analysis and obtain an average  $D_f$  for the particles from dry beech wood combustion of  $2.09 \pm 0.06$ .

##### 4.2.2. SEM pictures of biomass combustion particles

During the experiments on 03/06/18, the particles from the combustion of beech sticks were sampled on gold-coated membrane filters behind the DMA and the filters were analyzed using a scanning electron microscope (SEM). For details of the SEM analysis see Gwaze et al. [22]. Examples are shown in Fig. 8c and d. Particles from oak combustion were sampled on an earlier date without preselection with a DMA (Fig. 8a and b). Although the oak combustion particles are not spherical, they show a compact morphology and look markedly different from the fractal like aggregates that were found in the smoke from combustion of beech. This finding fits very well to the different aerodynamic behavior of the particles and to the different fractal dimensions inferred from our measurements.

##### 4.2.3. Comparison with previous results

For the same beech combustion experiments discussed above, Gwaze et al. [22] obtain an average  $D_{f,2}$  value of 1.83 (two-dimensional fractal dimension) derived from three different techniques based on 2D projections. However, from our method,  $D_f$  values lower than 2 cannot be inferred, since the data collected by the AMS-DMA combination would yield constant  $d_{va}$  values (independent of  $d_m$ ) if the fractal dimension is equal or lower than 2. It must be considered, however, that  $D_f < 2$  is inherent to any method looking at projections of irregular particles [19], as done by Gwaze et al. [22]. Furthermore,  $D_{f,2}$  is smaller by 10–15% (for  $D_{f,2} \approx 2$  as encountered here) than the value for  $D_f$  inferred from a three-dimensional method [51]. Increasing the  $D_{f,2}$  value reported by Gwaze et al. [22] by 10 and 15% yields

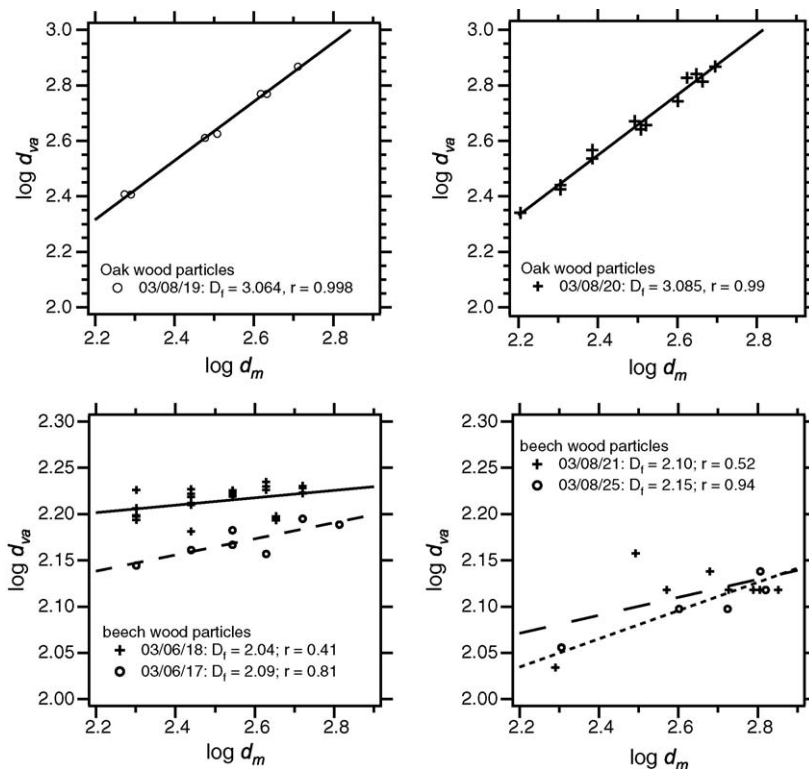


Fig. 7. Logarithms of vacuum aerodynamic diameter vs. mobility equivalent diameter for particles from oak and beech combustion. The linear regression curves yield the fractal dimension according to Eq. (10). The estimated fractal dimension  $D_f$  is about 3 for the oak particles and ranges between 2.04 and 2.15 for the beech particles. The beech data measured on 03/08/21 do not have sufficient statistical significance (see text).

2.01–2.10, respectively. This is in excellent agreement with our results.

Schmidt-Ott inferred a fractal dimension of 2.18 for Ag particles formed by homogeneous nucleation [19]. A fractal

dimension of 2.15 is the theoretical value for reaction-limited cluster aggregation [51]. Both values are very similar to our average  $D_f$  value of  $2.09 \pm 0.06$  for the beech combustion particles.

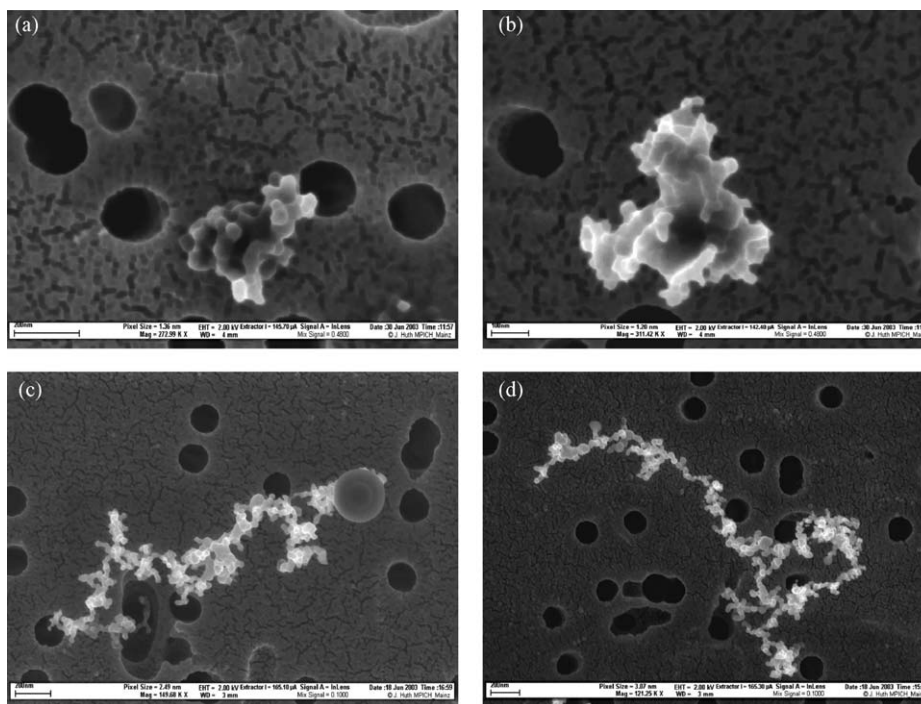


Fig. 8. SEM pictures of biomass combustion particles: (a and b) oak combustion particles (no preselection with DMA) and (c and d) beech combustion particles, 03/06/18—(c)  $d_m = 100$  nm and (d)  $d_m = 200$  nm.

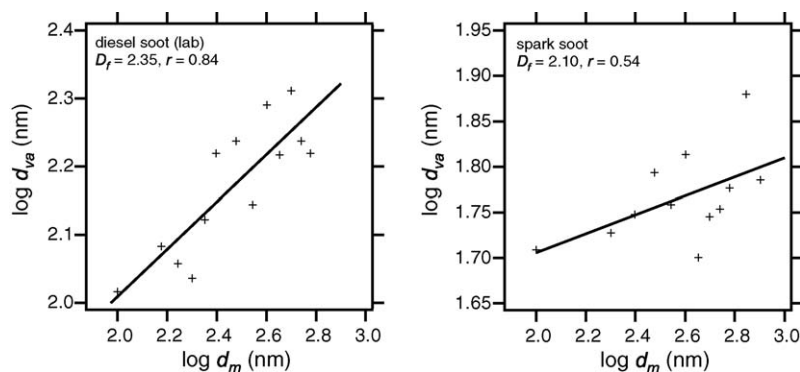


Fig. 9. Examples for further experiments with fractal-like particles: laboratory-generated diesel combustion particles (left panel) reveal a fractal dimension of 2.35; spark soot particles (PALAS GFG1000, right panel) reveal a fractal dimension of 2.10.

#### 4.2.4. Fractal dimension analysis of other combustion particles

Correlations of  $d_{va}$  and  $d_m$  for laboratory-generated diesel combustion particles and spark soot particles generated with the PALAS GFG1000 generator show similar results as biomass burning particles from beech sticks (Fig. 9). The undesired contamination of the spark soot particles due to the polyamide chamber of the generator and the conductive silicone tubing allows the determination of the aerodynamic diameter with the AMS. The particles from diesel combustion reveal a fractal dimension of  $2.35 \pm 0.07$ , while the spark soot particles reveal a fractal dimension of  $2.10 \pm 0.05$ . The error limits here are given by the standard deviation of the slope parameter during the fitting process. The positive correlation of the diesel combustion particles is significant within the 99% confidence level, while the correlation of the spark soot particles is only significant within a 90% confidence level. It was shown in Fig. 2 that the mass spectra of diesel exhaust particles and laboratory generated diesel combustion particles are very similar, but this is not necessarily the case for their shape. Park et al. [31] report fractal dimensions ranging from 2.3 to 2.8 for diesel engine exhaust particles from various engines under various conditions, which is in good agreement with the value we obtain for the laboratory combusted diesel particles. In a recent review paper, Burtscher [52] considers 2.3 a typical  $D_f$  value for diesel soot. In contrast, for soot particles produced by a propane flame, Slowik et al.

[24] found fractal dimensions of about 1.7, which is markedly smaller than our value.

For spark soot, a fractal dimension of 2.1 was also reported by Weingartner et al. [20]. In addition, Wentzel et al. [21] found a fractal dimension of 2.0 for spark soot particles based on their coagulation dynamics. Both values agree with our findings and imply that in our experiments the influence of the coating – originating from contamination – on the particle morphology is negligible.

#### 4.2.5. Effective density and shape factor

The effective density that was defined in Eq. (4) and parameterized in Eq. (6) can be fitted to the experimental data to obtain information on the particle density and dynamic shape factor (Fig. 10). The left panel shows the effective density  $\rho_{eff}$  as a function of the mobility diameter ( $d_m$ ) along with three fit curves: in the first curve (solid line), the dynamic shape factor ( $\chi$ ) was set to 1 (spherical particles), since this is the theoretical minimum value for  $\chi$  in the absence of alignment effects. The effective density is then a constant value, defined by the mean ratio between  $d_{va}$  and  $d_m$ , and equals the particle density  $\rho_p$ . Under these assumptions, the inferred bulk particle density is  $1.44 \text{ g cm}^{-3}$ . For the second fit curve (dotted line), the particle density was set to a constant value of  $2 \text{ g cm}^{-3}$ , since this is approximately the density of elemental carbon and is taken as an approximation for the upper limit for the density of the

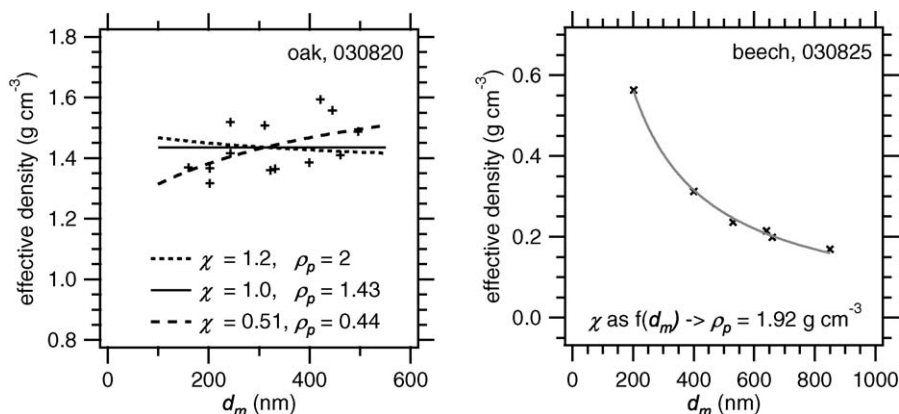


Fig. 10. Effective density as defined in Eq. (6), fitted to the experimental data for two examples of biomass burning particles (oak and beech).

oak combustion particles. Then, the effective density decreases with increasing  $d_m$ , and the resulting shape factor  $\chi$  is 1.2. Allowing also  $\chi$  values smaller than 1 (accounting for possible alignment effects), the best fit yields a  $\chi$  value of 0.51 and a very low bulk density of  $0.44 \text{ g cm}^{-3}$  (dashed line). This curve reproduces best the slight increase of the effective density with  $d_m$ .

The right panel of Fig. 10 shows the effective density of the beech combustion particles measured on 03/08/25. Since it has been observed frequently that the dynamic shape factor increases with  $d_m$  [22,24,53], we parameterized the dynamic shape factor as function of the mobility diameter  $\chi = a(d_m/d_{pp})^b$ , using the  $d_{pp}$  value of 51 nm as measured by Gwaze et al. [22]. By this, the experimental data could be reproduced well, yielding a bulk particle density of  $1.92 \text{ g cm}^{-3}$ . With the fitted values of 1.13 and 0.45 for the parameters  $a$  and  $b$ , respectively, the dynamic shape factor ranges between 2.1 (200 nm) and 4.1 (850 nm), which is higher by 20–60% than the values reported by Gwaze et al. [22] for the same experiment. The inferred density of  $1.92 \text{ g cm}^{-3}$  is in agreement with bulk densities that have been reported for other types of soot particles. Park et al. [54] found inherent densities between 1.7 and  $1.8 \text{ g cm}^{-3}$  for diesel soot particles with mobility diameters larger than 100 nm. However, no data on the density of biomass burning fractal particles have so far been reported. It might also be conceivable that the particle density is not constant but is a function of the mobility diameter. With the limited number of data points in this experiment, it was not possible to include such a functional dependence into the fit procedure.

## 5. Summary and conclusion

The mass spectrometric signatures of particles generated in various types of combustion processes were investigated using the aerodyne AMS (quadrupole version). Although this instrument cannot detect elemental carbon and has additional limitations in the analysis of organic compounds, namely unit resolution and fragmentation of the organic molecules upon flash evaporation and electron impact ionization, important conclusions on the chemical nature of the individual particle types could be inferred. The mass spectrometric data indicated that diesel engine exhaust particles closely resembled particles produced by laboratory diesel combustion and particles produced by evaporating and re-condensing lubrication oil. The similarity to nebulized diesel and nebulized lubrication oil was slightly smaller.

In the mass spectra of spark soot particles produced with the PALAS GFG soot generator, we found contamination originating most likely from the polyamide chamber of the generator and of the conductive silicone tubing ( $m/z$  73, 147, 207, 221, and 281). The silicone contamination signatures were also found in mass spectra from particles produced by an oxygen-poor flame in the laboratory, by a diesel engine, and partly also in biomass burning particles.

Biomass burning particles show signatures for levoglucosan:  $m/z$  73 ( $\text{C}_3\text{H}_5\text{O}_2^+$ ) and  $m/z$  60 ( $\text{C}_2\text{H}_4\text{O}_2^+$ ). Levoglucosan mass spectra recorded in the laboratory were found to have similar

ion ratios for these mass peaks as the NIST reference spectrum, suggesting that NIST reference spectra are a valid source for interpretation of AMS spectra. It can be ruled out that the  $m/z$  73 ion ( $\text{C}_3\text{H}_5\text{O}_2^+$ ) in the levoglucosan spectrum is the same mass fragment as the  $m/z$  73 signal that is related to silicone contamination ( $\text{SiOC}_2\text{H}_5^+$ ).

From the combination of the vacuum aerodynamic and the mobility diameter, some interesting findings regarding particle morphology were derived. The fractal dimension and thereby the aerodynamic behavior of different types of biomass burning was found to be significantly different, depending on the state of the biomass fuel. Particles derived from natural oak wood combustion revealed a fractal dimension  $D_f$  of about three, while particles from the combustion of dry beech wood had a fractal dimension of  $2.09 \pm 0.06$  (ranging between 2.04 and 2.15). This finding is consistent with SEM pictures showing the fractal nature of the beech combustion particles and the compact shapes of the oak combustion particles.

Similar results were found for other soot particles: particles from laboratory diesel combustion with an oxygen-poor flame had a fractal dimension of 2.35 and spark soot particles were found to have a  $D_f$  of 2.10. These results are in good agreement with previous measurements [20,31].

In addition, the dynamic behavior of compact particles from oak combustion suggested a lower limit for the particle (bulk) density of  $1.44 \text{ g cm}^{-3}$  for an assumed dynamic shape factor of 1, and an upper limit for the shape factor of 1.2 was inferred by setting the particle density to 2.0, a value that is reported for black carbon and might be representative as an upper limit for the density of biomass burning particles. Allowing also values smaller than 1 for the shape factor, thereby accounting for possible alignment effects in the aerodynamic lens of the mass spectrometer, the data were best reproduced with values for the shape factor of 0.5 and for the bulk density of  $0.44 \text{ g cm}^{-3}$ , both of which can be regarded as unrealistically low.

The fractal-like particles could also be described with a dynamic shape factor that is a function of the mobility diameter, similar to the finding of Gwaze et al. [22]. This means that the particles become less compact with increasing size and experience a higher drag force. This finding had been reported also by Park et al. [53] for diesel exhaust particles, and by Gwaze et al. [22] for particles collected in the same experiments as the data presented here.

The inferred density of the fractal like particles from beech combustion is  $1.92 \text{ g cm}^{-3}$ . This value is in the range of previously published data on diesel soot, however, no other data on the density of airborne biomass burning particles are available.

The differences between the particles produced from combustion of dry beech sticks and natural state biomass fuel (especially from oak combustion) are reflected in the mass spectrometric data (Fig. 5) as well as in the data on particle morphology (Fig. 6). It is conceivable that biomass burning particles from natural wood (e.g., forest fires) or other natural biomass fuel with higher water content are more likely to resemble the particles from oak combustion in our experiments, while particles produced by modern wood-based heating systems resemble the

particles from the dry beech stick combustion. The influence of these differences in biomass fuel conditions on the properties of the generated particles have to be accounted for when interpreting and comparing biomass burning particles in different locations in the world.

### Acknowledgments

We acknowledge the various contributions by T. Böttger, S.S. Hings, N. Hock, J. Huth, G. Frank, U. Dusek (MPI for Chemistry), and V. Scheer (Ford Forschungszentrum) to the measurements, and the comments by M. Kamphus (University Mainz). We also thank one of the reviewers for comments that helped identifying the silicone tubing contamination.

### References

[1] M.Z. Jacobson, *J. Geophys. Res.* 107 (D19) (2002) 4410, doi:10.1029/2001JD001376.  
[2] W.L. Chameides, M. Bergin, *Science* 297 (2002) 2214.  
[3] P. Guyon, B. Graham, J. Beck, O. Boucher, E. Gerasopoulos, O.L. Mayol-Bracero, G.C. Roberts, P. Artaxo, M.O. Andreae, *Atmos. Chem. Phys.* 3 (2003) 951.  
[4] J.E. Penner, S.Y. Zhang, C.C. Chuang, *J. Geophys. Res.* 108 (D21) (2003) 4657, doi:10.1029/2003JD003409.  
[5] M.O. Andreae, D. Rosenfeld, P. Artaxo, A.A. Costa, G.P. Frank, K.M. Longo, M.A.F. Silva-Dias, *Science* 303 (2004) 1337.  
[6] A. Peters, H.E. Wichmann, T. Tuch, J. Heinrich, J. Heyder, *Am. J. Respir. Crit. Care Med.* 155 (1997) 1376.  
[7] C.A. Pope 3rd, *J. Aerosol Med.* 13 (2000) 335.  
[8] H. Schulz, V. Harder, A. Ibaldo-Mulli, A. Khangdoga, W. Koenig, F. Krombach, R. Radykewicz, A. Stampfl, B. Thorand, A. Peters, *J. Aerosol Med.* 18 (2005) 1.  
[9] G. Oberdörster, *Int. Arch. Occup. Environ. Health* 74 (2001) 1.  
[10] B. Asgharian, W. Hofmann, R. Bergmann, *Aerosol Sci. Technol.* 34 (2001) 332.  
[11] H.-E. Wichmann, C. Spix, Th. Tuch, G. Wölke, A. Peters, J. Heinrich, W.G. Kreyling, J. Heyder, *Daily Mortality and Fine and Ultrafine Particles in Erfurt, Germany Part I: Role of Particle Number and Particle Mass*, Health Effects Institute, Cambridge, MA, Research Report No. 98, 2000.  
[12] M.R. Canagaratna, J.T. Jayne, D.A. Ghertner, S. Herndon, Q. Shi, J.L. Jimenez, Ph.J. Silva, P. Williams, Th. Lanni, F. Drewnick, K.L. Demerjian, Ch.E. Kolb, D.R. Worsnop, *Aerosol Sci. Technol.* 38 (2004) 555.  
[13] J. Schneider, B.N. Hock, S. Weimer, S. Borrmann, U. Kirchner, R. Vogt, V. Scheer, *Environ. Sci. Technol.* 39 (2005) 6153.  
[14] W.F. Rogge, L.M. Hildemann, M.A. Mazurek, G.R. Cass, *Environ. Sci. Technol.* 27 (1993) 636.  
[15] W.F. Rogge, L.M. Hildemann, M.A. Mazurek, G.R. Cass, B.R.T. Simoneit, *Environ. Sci. Technol.* 32 (1998) 13.  
[16] J.S. Reid, R. Koppmann, T.F. Eck, D.P. Eleuterio, *Atmos. Chem. Phys.* 5 (2005) 799.  
[17] S. Decesari, S. Fuzzi, M.C. Facchini, M. Mircea, L. Emblico, F. Cavalli, W. Maenhaut, X. Chi, G. Schkolnik, A. Falkovich, Y. Rudich, M. Claeys, V. Pashynska, G. Vas, I. Kourtev, R. Vermeylen, A. Hoffer, M.O. Andreae, E. Tagliavini, F. Moretti, P. Artaxo, *Chem. Phys.* 6 (2006) 375.  
[18] S. Fuzzi, S. Decesari, M.C. Facchini, F. Cavalli, L. Emblico, M. Mircea, et al., Overview of the inorganic and organic composition of size-segregated aerosol in Rondônia, Brazil, from the biomass burning period to the onset of the wet season. *J. Geophys. Res.*, 2006, in press.  
[19] A. Schmidt-Ott, *Appl. Phys. Lett.* 52 (1988) 954.  
[20] E. Weingartner, U. Baltensperger, H. Burtscher, *Environ. Sci. Technol.* 29 (1995) 2982.  
[21] M. Wentzel, H. Gorzawski, K.-H. Naumann, H. Saathoff, S. Weinbruch, *J. Aerosol Sci.* 34 (2003) 1347.

[22] P. Gwaze, O. Schmid, H.J. Annegarn, M.O. Andreae, J. Huth, G. Helas, *J. Aerosol Sci.* 37 (2006) 820, doi:10.1016/j.jaerosci.2005.06.007.  
[23] P.F. DeCarlo, J.G. Slowik, D.R. Worsnop, P. Davidovits, J.L. Jimenez, *Aerosol Sci. Technol.* 38 (2004) 1185.  
[24] J.G. Slowik, K. Stainken, P. Davidovits, L.R. Williams, J.T. Jayne, C.E. Kolb, D.R. Worsnop, Y. Rudich, P.F. DeCarlo, J.L. Jimenez, *Aerosol Sci. Technol.* 38 (2004) 1206.  
[25] J.L. Jimenez, R. Bahreini, D.R. Cocker III, H. Zhuang, V. Varutbangkul, R.C. Flagan, J.H. Seinfeld, C.D. O'Dowd, T. Hoffmann, *J. Geophys. Res.* 108 (D10) (2003) 4318, doi:10.1029/2002JD002452.  
[26] W.C. Hinds, *Aerosol Technology: Properties, Behaviour, and Measurement of Airborne Particles*, Wiley and Sons, New York, 1999.  
[27] M.D. Allan, O.G. Raabe, *J. Aerosol Sci.* 13 (1982) 537.  
[28] J.L. Jimenez, R. Bahreini, D.R. Cocker III, H. Zhuang, V. Varutbangkul, R.C. Flagan, J.H. Seinfeld, C.D. O'Dowd, T. Hoffmann, *J. Geophys. Res.* 108 (D23) (2003) 4733, doi:10.1029/2003JD004249.  
[29] S.K. Friedlander, *Smoke Dust, and Haze: Fundamentals of Aerosol Dynamics*, Oxford University Press, New York, 2000.  
[30] A. Schmidt-Ott, U. Baltensperger, H.W. Gäggeler, D.T. Jost, *J. Aerosol Sci.* 21 (1990) 711.  
[31] K. Park, D.B. Kittelson, P.H. McMurry, *Environ. Sci. Technol.* 37 (2003) 577.  
[32] C. van Gulijk, J.C.M. Marijnissen, M. Makkee, J.A. Moulijn, A. Schmidt-Ott, *J. Aerosol Sci.* 35 (2004) 633.  
[33] J.T. Jayne, D.C. Leard, X. Zhang, P. Davidovits, K.A. Smith, C.E. Kolb, D.R. Worsnop, *Aerosol Sci. Technol.* 33 (2000) 49.  
[34] J.L. Jimenez, J.T. Jayne, Q. Shi, C.E. Kolb, D.R. Worsnop, I. Yourshaw, J.H. Seinfeld, R.C. Flagan, X. Zhang, K.A. Smith, J. Morris, P. Davidovits, *J. Geophys. Res.* 108 (2003) 8425, doi:10.1029/2001JD001213.  
[35] J.D. Allan, J.L. Jimenez, P.I. Williams, M.R. Alfarra, K.N. Bower, J.T. Jayne, H. Coe, D.R. Worsnop, *J. Geophys. Res.* 108 (2003) 4090, doi:10.1029/2002JD002358.  
[36] J.D. Allan, A.E. Delia, H. Coe, K. Bower, M.R. Alfarra, J.L. Jimenez, A.M. Middlebrook, F. Drewnick, T.B. Onasch, M.R. Canagaratna, J.T. Jayne, D.R. Worsnop, *J. Aerosol Sci.* 35 (2004) 909.  
[37] C. Helsper, W. Mölter, F. Löffler, C. Wadenpohl, S. Kaufmann, G. Wenninger, *Atmos. Environ.* 27A (1993) 1271.  
[38] C. Roth, G.A. Ferron, E. Karg, B. Lentner, G. Schumann, S. Takenaka, J. Heyder, *Aerosol Sci. Technol.* 38 (2004) 228.  
[39] Y. Iinuma, E. Brüggemann, T. Gnauk, M. O. Andreae, G. Helas, K. Müller, et al., Source characterization of biomass burning particles: The combustion of European conifers, African hardwood, savanna grass, and German and Indonesian peat, *J. Geophys. Res.*, 2006, in press.  
[40] V. Scheer, U. Kirchner, R. Casati, R. Vogt, B. Wehner, S. Philippin, A. Wiedensohler, N. Hock, J. Schneider, S. Weimer, S. Borrmann, *SAE Technical Paper Series 2005-01-0197* (2005).  
[41] F.W. McLafferty, F. Turecek, *Interpretation of Mass Spectra*, 4th ed., University Science Books, Sausalito, CA, 1993.  
[42] H.J. Tobias, D.E. Beving, P.J. Ziemann, H. Sakurai, M. Zuk, P.H. McMurry, D. Zarling, R. Watlylonis, D.B. Kittelson, *Environ. Sci. Technol.* 35 (2001) 2233.  
[43] H. Sakurai, H.J. Tobias, K. Park, D. Zarling, K.S. Docherty, D.B. Kittelson, P.H. McMurry, P.J. Ziemann, *Atmos. Environ.* 37 (2006) 1199.  
[44] F. Liang, M. Lu, T.C. Keener, Z. Liu, S.-J. Khang, *J. Environ. Monit.* 7 (2005) 983.  
[45] NIST Mass Spectrometry Data Center, Collection © 2002 copyright by the U.S. Secretary of Commerce on behalf of the United States of America, 2002.  
[46] M.R. Alfarra, *Insights into Atmospheric Organic Aerosols Using an Aerosol Mass Spectrometer*, Ph.D. Dissertation Thesis, University of Manchester, Manchester, 2004.  
[47] R. Bahreini, M. Keywood, N.L. Ng, V. Varutbangkul, S. Gao, R.C. Flagan, J.H. Seinfeld, D.R. Worsnop, J.L. Jimenez, *Environ. Sci. Technol.* 39 (2005) 5674, doi:10.1021/es048061a.  
[48] J. Schneider, S. Borrmann, A.G. Wollny, M. Bläsner, N. Mihalopoulos, K. Oikonomou, J. Sciare, A. Teller, Z. Levin, D.R. Worsnop, *Atmos. Chem. Phys.* 4 (2004) 65.

- [49] Q. Zhang, M.R. Alfarra, D.R. Worsnop, J.D. Allan, H. Coe, M.R. Canagaratna, J.L. Jimenez, *Environ. Sci. Technol.* 39 (2005) 4938, doi:10.1021/es048568l.
- [50] N. Takegawa, Y. Miyazaki, Y. Kondo, Y. Komazaki, T. Miyakawa, J.L. Jimenez, J.T. Jayne, D.R. Worsnop, J.D. Allan, R.J. Weber, *Aerosol Sci. Technol.* 39 (2005) 760.
- [51] P.A. Baron, K. Willeke, *Aerosol Measurement: Principles, Techniques, and Applications*, Wiley and Sons, New York, 2001.
- [52] H. Burtscher, *J. Aerosol Sci.* 36 (2005) 896.
- [53] K.D. Park, B. Kittelson, P.H. McMurry, *Aerosol Sci. Technol.* 38 (2004) 881.
- [54] K.D. Park, B. Kittelson, P.H. McMurry, *J. Nanopart. Res.* 6 (2004) 267.